Synthesis, characterization, antibacterial and antifungal properties of ZnO and Ag doped ZnO nanoparticles

T. MALAERU[1], C. MORARI[1,*], N. O. NICULA[1], B. G. SBARCEA[1], V. MARINESCU[1], A. CUCOS[1], A. MOANTA[2], G. GEORGESCU[1], C. A. BANCIU[1,*]
[1]*National Institute for Research and Development in Electrical Engineering ICPE-CA Bucharest, 313 Splaiul Unirii, 030138, Bucharest 3, Romania*
[2]*CEPROCIM SA, Street Preciziei, No. 6, Bucharest 6, Romania*

ZnO nanoparticles (NPs) have proven over time to have high applicability in the fields of optics, optoelectronics, sensors, supercapacitors, and nanomedicine. In this work, the ZnO and Ag-doped ZnO NPs were prepared by a modified sol-gel method at 60°C in the presence of sodium dioctyl sulfosuccinate (DOSS) as a surfactant and xylitol as the gelling agent. All the synthesized samples have a hexagonal wurtzite structure with a crystallite size of 34.4 nm–50.4 nm and a rod-like morphology. The ZnO sample has the largest inhibition zone diameter of 4.17 cm (at *S. aureus*), while the 5% wt. Ag-doped ZnO sample has a diameter of 3.03 cm (at *E. coli*). The 0.3 and 0.5% wt. Ag-doped ZnO samples have a high resistance to the action of fungi (after 28 days).

(Received October 27, 2023; accepted February 12, 2024)

Keywords: ZnO nanoparticles, Sol-gel method, Antibacterial, Antifungal

1. Introduction

Lately, the increase in demand for NPs-based products in various industrial fields has led to an increase in the need for NPs with specific characteristics designed through various synthesis techniques and methods [1-4].

Among the many metallic oxide nanoparticles, ZnO NPs have seen increasing demand for applications in industries such as energy, textiles, food, cosmetics, drugs, and nanomedicine [5-9].

ZnO nanostructures, due to their semiconducting, piezoelectric, photoluminescence and pyroelectric properties, have proven to have high applicability in the field of optics, optoelectronics, sensors and supercapacitors [10-14].

Also, ZnO NPs, a semiconductor material with a wide bandgap of 3.37 eV and a large excitonic binding energy of 60 meV, which give them photo-oxidizing and photocatalytic properties [2], have been widely used as antimicrobial agents [15].

Although the antibacterial mechanism of ZnO nanoparticles is not fully elucidated, the following three mechanisms have been proposed: the formation of reactive oxygen species (ROS), the interaction of nanoparticles with bacteria leading to damage to the bacteria, and the release of Zn^{2+} [16].

Their antimicrobial properties can be improved by modifying the following characteristics: composition, size, morphology, surface defects and functionalization.

On the other hand, ZnO is a cheap, biocompatible, non-toxic material for the human cell with high photochemical and thermal stability that can be obtained with low production costs through numerous chemical methods in solution, such as co-precipitation [17], sol-gel [18-21], microemulsions [22], hydrothermal [23], and solvothermal [24].

Among the many methods for the preparation of ZnO NPs, the sol-gel method is one of the most promising because it presents several advantages, such as: it is an easy method that allows composition control, obtaining compounds with high purity; it requires low decomposition temperatures; simple installations; low cost; energy efficiency; and a high yield of production.

The sol-gel method has received an increased attention in last decade in an attempt to synthesize nanostructured ZnO (including nanodots, nanorods, nanobelts, nanotubes, nanoflowers), a versatile functional material, and to exploit its properties which are promising for incorporating it into optoelectronic devices [25].

The sol-gel method is a simple, environmentally friendly method that has the ability to control the size and morphology of the particles by controlling the reaction parameters such as the type of precursor, the concentration of the reactants, the solvent and the type of dopant, the pH of the reaction medium and annealing temperature.

In the paper [26], ZnO nanoparticles resembling thorns with different sizes were prepared by the sol-gel method using zinc acetate dihydrate (ZnAc) as a precursor and cetyltrimethylammonium bromide (CTAB) as a surfactant in an aqueous medium at different stirring speeds. The results showed that the stirring speed, probably by inducing the internal shear force, has an impact on the size and morphology of the ZnO nanoparticles.

Y.K. Tseng et al. report the synthesis of ZnO nanostructures using a sol-gel method with zinc acetate dihydrate as a solute, and different polyols as solvents. After hydrolysis at 160°C, the zinc alkoxide particles self-assembled into polycrystalline nanostructures with different morphologies (fibers, rhombic flakes, spheres) [27].

In [28], the effect of the precursor on the morphology and size of ZnO nanoparticles prepared by a sol-gel method is shown. The use of zinc nitrate as a precursor led to obtaining ZnO NPs with an almost spherical morphology and a particle mean size of 99.28 nm, while by using zinc acetate, rod-like nanoparticles with a size of 40.94 nm were obtained.

Another way to increase the antibacterial activity of ZnO NPs consist in their doping. Thus, the impurity atoms that enter the ZnO network regulate the physico-chemical properties and increase the antibacterial activity [29].

K. Ravichandran et al. report that in the case of doping ZnO with Mn in an amount of 10% wt., the antibacterial efficiency against the *E. coli* bacteria increases [30]. Likewise, N. M. Khatir et al. reported the synthesis of Fe-doped ZnO NPs with magnetic properties and antibacterial activity [31]. Also, ZnO NPs doped with Ag prepared by a hydrothermal method showed increased antibacterial activity compared to pure ZnO [32].

In [33] the authors investigated the antibacterial and antifungal activity of Ag-ZnO nanocomposites (synthesized from fenugreek leaf extract) against Gram-positive *Staphylococcus aureus*, Gram-negative bacteria *Escherichia coli* and fungi *Candida albicans*. The inhibition zone diameters of both bacteria and *Candida albicans* were measured by the disk diffusion method. The results showed that the synthesized Ag-ZnO nanocomposites had less influence on *E. coli* compared to *S. aureus*.

In this article we present the synthesis of ZnO and Ag-doped ZnO NPs by a sol-gel method in the presence of an anionic surfactant - DOSS and a gelling agent sugar alcohol (Xylitol) at low temperature (60°C). The synthesis approach is simple, economical, and reproducible on an industrial scale. We also present the synergistic effect of the dopant ion (Ag+) concentration and organic coating on the surface of the nanoparticles on the antibacterial and antifungal resistance and efficiency of synthesized samples.

2. Experimental

2.1. Materials

In this work, for the synthesis of ZnO and Ag doped ZnO NPs by the sol-gel technique, the following chemical substances of analytical purity were used: zinc acetate dihydrate [$Zn(CH_3COO)_2{\cdot}2H_2O$] (98% purity) from Sigma Aldrich and silver nitrate ($AgNO_3$) of 99% purity purchased from CRISTAL R. CHIM SRL as precursors, the basic catalyst sodium hydroxide (NaOH) pellets (from Sigma Aldrich), double-distilled water (H_2O D.D.) and ethanol $(C_2H_5)OH$ (99.5%, from Sigma Aldrich) as solvents, DOSS (>96%) from Thermo Scientific as a surfactant, and xylitol (99% purity, from Sigma Aldrich) as a gelling agent.

2.2. Synthesis of ZnO and Ag doped ZnO NPs via sol-gel method

The zinc acetate di-hydrate ($Zn(CH_3COO)_2{\cdot}2H_2O$) used as a precursor, in the quantities specified for each sample synthesized in Table 1, was dissolved in a mixture consisting of 250 ml H_2O D.D. and 750 ml ethyl alcohol by magnetic stirring (1200 rpm) and heating at 40°C for 20 min. The silver nitrate used as a dopant in the amounts specified in Table 1 was dissolved in 100 ml of H_2O D.D. and then added over the zinc acetate solution. Then an anionic surfactant solution formed by dissolving 0.01mol (4.45 g) DOSS in 250 ml H_2O D.D. was added to the mixture of the two solutions, and the magnetic stirring continued for another 15 min. After that, the gelling agent solution formed by dissolving 0.015 mol (2.2822 g) of xylitol in 200 ml of H_2O D.D. was added to the solution mixture thus formed. Stabilization of the working pH of the reaction system at a value of 10 was achieved by adding dropwise a 2M NaOH solution.

Table 1. The composition and coding of synthesized samples

Sample coding	Sample composition	
	$Zn(CH_3COO)_2{\cdot}H_2O$	$AgNO_3$
ZnO	1 mol (219.5 g)	-
0.3% wt. Ag-doped ZnO	0.997 mol (218.8415 g)	0.003 mol (0.5096 g)
0.5% wt. Ag-doped ZnO	0.995 mol (218.4025 g)	0.005 mol (0.8493 g)
0.7% wt. Ag-doped ZnO	0.993 mol (217.9635 g)	0.007 mol (1.1890 g)

The reaction mixture was further kept at a constant temperature of 60°C with magnetic stirring (1200 rpm) for 2 h. After the end of the reaction, the mixture was left to age for 2 days and then separated by centrifugation at a speed of 6000 rpm for 15 min. The precipitate, separated by centrifugation, was washed twice with H_2O D.D. and finally with absolute ethyl alcohol and dried in an oven at 100°C for 2 h.

2.3. Characterization

To identify the crystalline phase and estimate the average size of the crystallite, a Bruker-AXS type D8 X-ray diffractometer was used with the following technical analysis conditions: X-ray tube with Cu anode, 40 kV/40 mA, 1D LynxEye detector, angular increment: 0.04°, angular measuring range: 2θ=10°-100°. Infrared spectra were recorded on a FTIR Bruker Tensor 27 spectrophotometer, in transmission mode using KBr pellets, by performing 32 scans in the 4000-280 cm^{-1} wavenumber range at 2 cm^{-1} resolution. The surface morphology and size of the thus synthesized NPs were

observed by a FESEM-FIB Scanning Electron Microscope (Workstation Auriga) equipped with a dispersive X-ray spectroscope detector (Oxford Instruments). Elemental compositions were determined by analysing an area through Energy-dispersive X-ray spectroscopy (EDX).

2.4. Antibacterial activity testing

Antibacterial activity testing of pure ZnO and Ag-doped ZnO powders was performed by a qualitative method using an adapted version of the Kirby Bauer disk diffusion method, according to the CLSI (2020) standard.

From each tested bacterial strain (*Staphylococcus aureus* ATCC 9737–*S. aureus* and *Escherichia coli* ATCC 25922–*E. coli*), a cell suspension was prepared in sterile distilled water (ADS) with a density of 0.5 MFarland ($1.5x10^8$ CFU/ml). Microbial suspensions (200 µl/plate) were seeded on solid Muller-Hinton (MH) medium, a medium conducive to the development of the bacteria used in the test. The plates were left at room temperature for 5 minutes, and afterwards, the powder samples were added, each with a diameter size of approximately 1 cm and a weight of 50 mg ± 5 mg.

The samples were incubated at 37°C for 24 hours. After incubation, the diameter of the growth inhibition zone (cm) was evaluated to determine the antibacterial effect of the tested powders (the diameter of the inhibition zone also includes the diameter of the tested sample; the shown value is the average of three values plus the related standard deviation of the average). All tests were performed in triplicate, with a blank represented by the medium inoculated with the bacterial strain used in the experiments.

2.5. Antifungal activity testing

The antifungal efficiency of the samples synthesized in this work was evaluated according to a method adapted according to SR EN 60068-2-10/2006 - Environmental testing – Part 2: Tests - Test J and guidance: Mould growth, and a method adapted according to ASTM G21-09 – Standard Practice for Determining Resistance of Synthetic Polymeric Materials to Fungi, 2009.

The powder samples (approx. 50 mg ± 5 mg, a diameter size of approx. 1 cm) were placed in Petri dishes containing a medium (Czapek-Dox Agar) conducive to the development of fungal strains. 0.1 ml of fungal spore suspension (consisting of a mixture of *Aspergillus brasiliensis* – ATCC 9642, *Penicillium funiculosum* – ATCC 11797, *Chaetomium globosum* – ATCC 6205, *Trichoderma virens* – ATCC 9645, and *Aureobasidium pullulans* – ATCC 15233) was added to the surface of the medium. The samples were incubated for 28 days at 28 ± 2°C and 95% relative humidity. To determine the resistance to the action of fungi, or the antifungal effect, every 7 days of the incubation period, the samples were evaluated visually and with a stereomicroscope. The presence of a zone of inhibition indicates antifungal properties. The degree of growth, depending on the degree of surface coverage of the samples, is scored on a scale of 0 to 4, with 0 indicating no growth and 4 indicating strong growth covering the entire surface of the sample. Materials with a grade of 0 to 1 are considered resistant to the action of fungi, while materials with a grade of 2 to 4 are considered not resistant to the action of fungi.

2.6. Statistical analysis

The experiments were conducted three times, and the findings were expressed as the mean ± standard deviation (SD) derived from three separate trials. Statistical significance was assessed using Student's t-test, considering a significance level of $p < 0.05$. The statistical analysis was carried out using Microsoft Excel 2021 software.

3. Results and discussion

3.1. X-ray diffraction (XRD) characterization

All XRD spectra recorded on the undoped and Ag-doped ZnO samples, prepared by the surfactant-assisted sol-gel process, showed a highly crystalline structure. The X-ray diffractogram presented in Fig. 1(a) showed that all the diffraction peaks associated with the catalogue sheet (PDF 00-001-1136) correspond to pure ZnO crystallized in a hexagonal system with a wurtzite structure. Also, the diffractograms in Fig. 1(b-d) showed the formation of Ag-doped ZnO with a hexagonal wurtzite structure, according to PDF 00-001-1136 and PDF 01-071-6424. In none of the X-ray diffractograms, the presence of another impurity phase was highlighted.

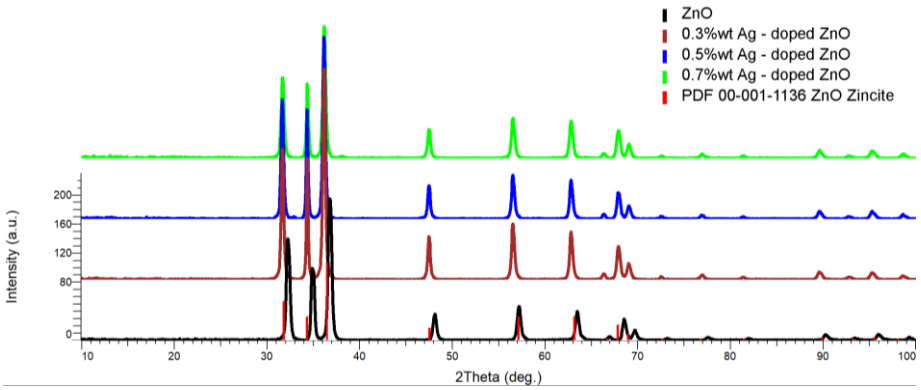

Fig. 1. The XRD patterns recorded on the samples of ZnO and Ag-doped ZnO NPs prepared by the surfactant-assisted sol-gel method (color online)

The average crystallite size and the parameters of the elementary cell, determined by Rietveld analysis for all analysed samples, are presented in Table 2.

The values of the lattice parameters for the samples of Ag-doped ZnO are slightly higher compared to those of undoped ZnO. Likewise, the values of the lattice parameters increase with the increase in the concentration of Ag^+ dopant ions. This increase indicates the incorporation of Ag at the Zn site.

Table 2. The value of the crystallite size and cell parameters for samples of ZnO and Ag-doped ZnO NPs

Sample	Crystallite size (nm)	Cell parameters	
		a (Å)	b (Å)
ZnO	34.4	3.243	5.195
0.3% wt. Ag-doped ZnO	50.4	3.245	5.198
0.5% wt. Ag-doped ZnO	47.4	3.246	5.199
0.7% wt. Ag-doped ZnO	37.9	3.249	5.204

3.2. FTIR characterization

The FTIR analysis was performed in order to determine the structure and groups existing on the surface of the ZnO and Ag-doped ZnO nanoparticles. Fig. 2 shows the FTIR spectra recorded on the ZnO and Ag-doped ZnO powder samples as they were prepared.

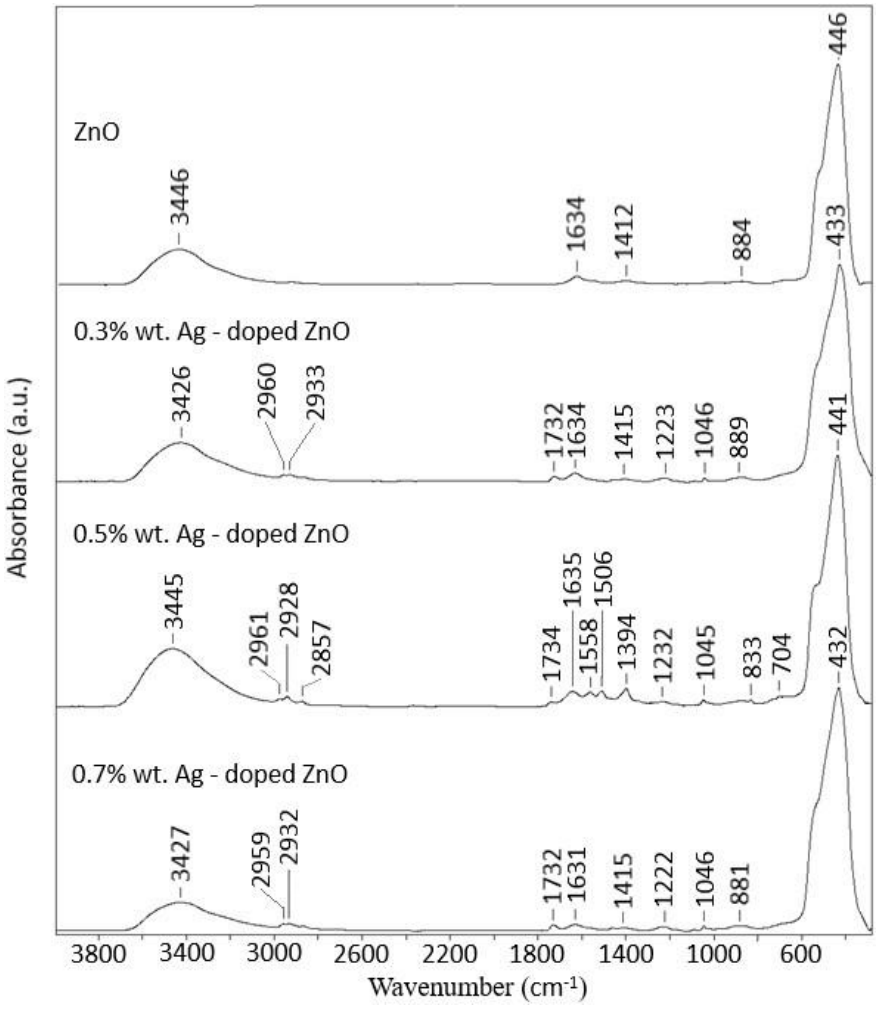

Fig. 2. The FTIR spectra recorded on the ZnO and Ag-doped ZnO powder samples

The high-intensity peaks at 445, 432, and 441 cm^{-1} correspond to the stretching vibrations of the Zn-O bonds in the ZnO structure. A slight shift of the band towards an inferior wavelength can be observed due to the partial substitution of the Ag^+ ion in the ZnO network [28].

The assignments of the characteristic groupings of the infrared bands are given in Table 3.

Table 3. The assignments of the characteristic groupings of the infrared bands

Wavenumber (cm^{-1})	Assignment
3447 – 3425	-OH stretching vibration
2961 – 2959	-CH_2 symmetric stretching vibration
2933 – 2857	-CH_2 asymmetric stretching vibration
1734 – 1731	C=O stretching vibration
1640 – 1631	COO asymmetric stretching vibration
1223 – 1223	In plane C-H bending
1046 – 1045	C-O-C stretching vibration
887 – 833	C-H bending
705 – 704	C-H rocking band
445 – 432	Zn-O stretching vibration

The groups identified by FTIR analysis were attributed to the organic compounds (surfactant and gelling agent) used in the synthesis and remaining on the surface of nanoparticles.

3.3. SEM and EDX characterization

The results of the SEM analysis, used to highlight the morphology and size of ZnO and Ag-doped ZnO nanoparticles, are shown in Fig. 3.

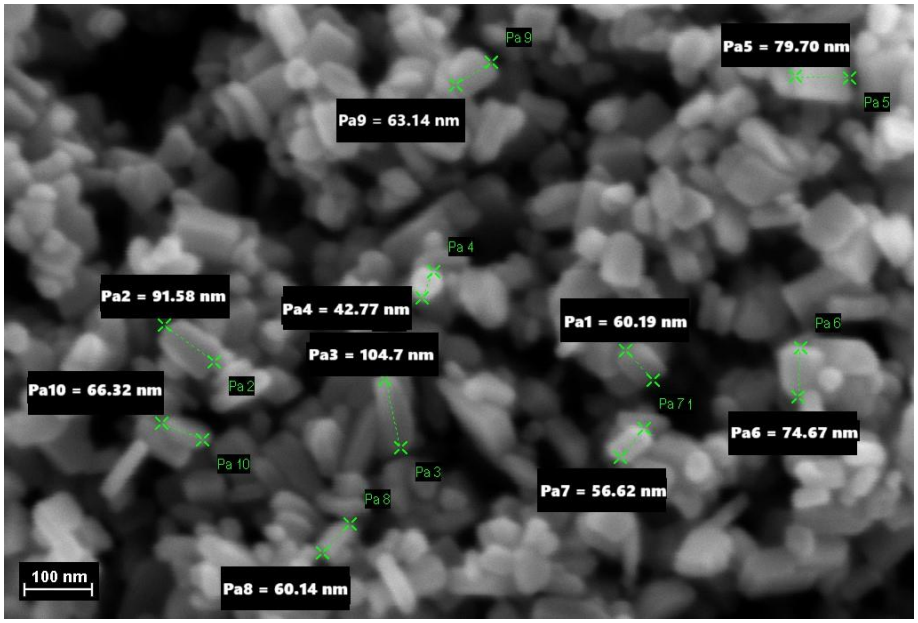

(a)

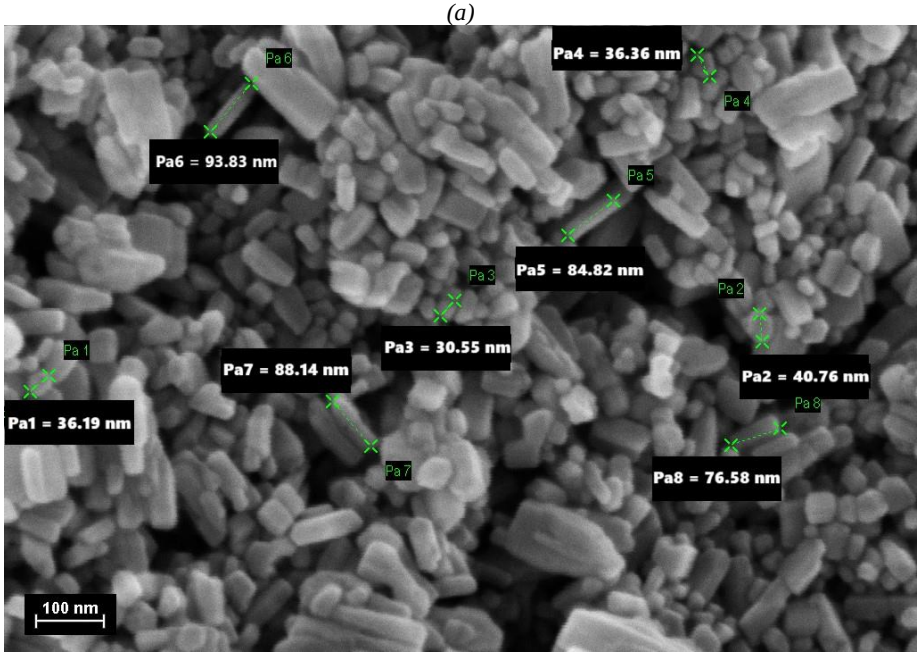

(b)

Fig. 3. SEM images of the samples: (a) ZnO; (b) 0.3% wt. Ag-doped ZnO; (color online)

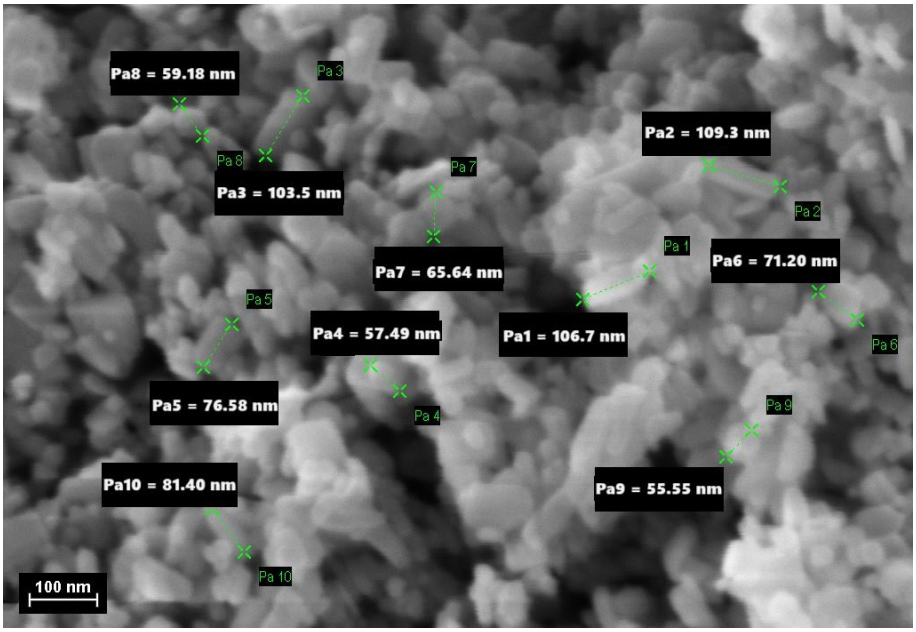

(c)

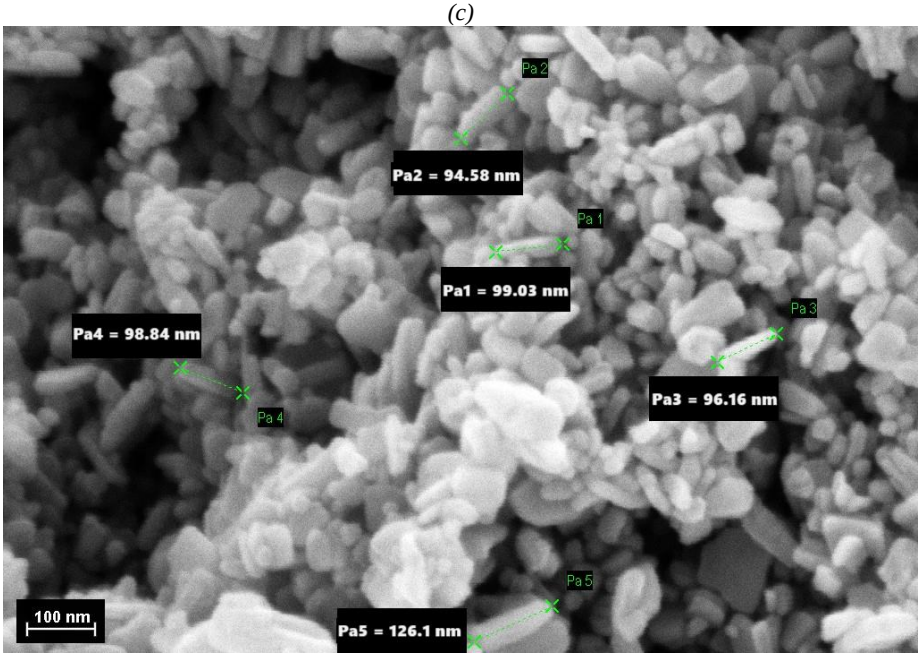

(d)

Fig. 3. (continued) SEM images of the samples: (c) 0.5% wt. Ag-doped ZnO; (d) 0.7% wt. Ag-doped ZnO (color online)

All samples showed agglomerations of particles with rod-like morphology and different rod lengths. The ZnO sample doped with 0.3% wt. Ag presented the smallest dimensions, with the length of the rod varying in the range of 36.19 - 93.83 nm. With the increase of the dopant content (at 0.7% Ag), the length of the rods increases to 94.58 - 126.1 nm (Fig. 3(d)).

The results of multipoint EDX analysis on the synthesized powder samples are shown in Fig. 4(a-d).

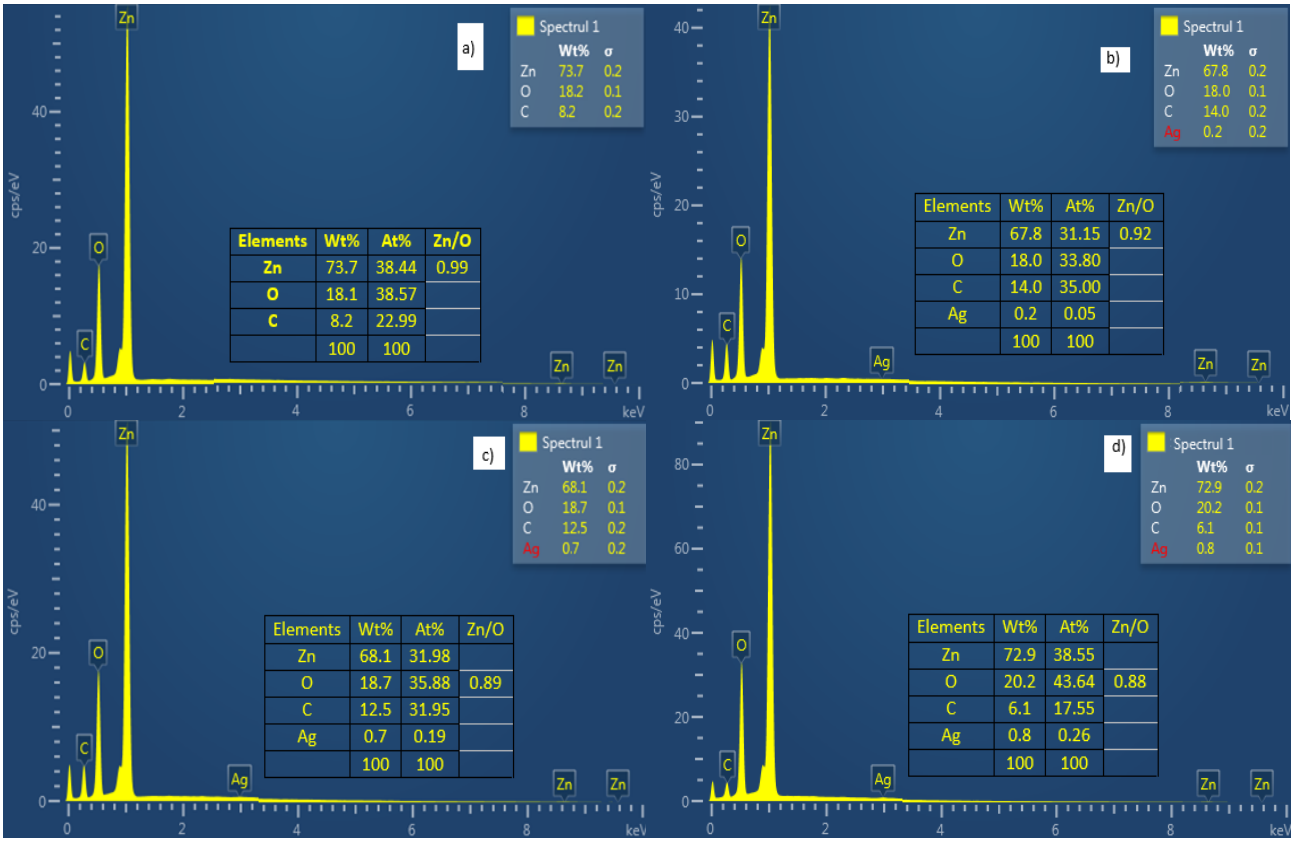

Fig. 4. EDX spectra of the samples: (a) ZnO; (b) 0.3% wt. Ag-doped ZnO; (c) 0.5% wt. Ag-doped ZnO; (d) 0.7% wt. Ag-doped ZnO (color online)

The EDX spectrum presented in Fig. 4(a) shows that the undoped ZnO sample is composed of the elements Zn, O, and C, the result being in agreement with the XRD and FTIR results. Also, the EDX spectra for the samples of ZnO doped with different amounts of Ag shown in Fig. 4(b-d) additionally highlight the presence of the Ag element, which supports the doping of ZnO with Ag^+ ions. In the case of undoped ZnO, Zn/O ratio value is 0.99 (close to 1, the theoretical value for ZnO), which means that a pure ZnO phase is formed. For the Ag-doped ZnO, the Zn/O ratio value is smaller than 1, which confirms the substitution of Zn^{2+} with Ag^+ and the formation of the $Zn_{1-x}Ag_xO$ phase.

3.4. Antibacterial characterization

The antibacterial efficiency of the ZnO and Ag-doped ZnO powder samples tested on the bacterial strains *S. aureus* and *E. coli*, proven by the clear inhibition zone, is shown in Table 4.

Table 4. Images of the inhibition zones (the halos around samples) showing the antibacterial effect of ZnO and Ag-doped ZnO powder samples on the tested strains, S. aureus and E. coli (color online)

Sample coding	***S. aureus* ATCC 9737**	***E. coli* ATCC 25922**
ZnO	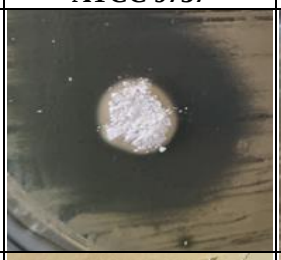	
0.3% wt. Ag-doped ZnO		
0.5% wt. Ag-doped ZnO		
0.7% wt. Ag-doped ZnO		

The inhibition zone values according to the tested strains and the analysed samples are shown in Table 5.

The antibacterial activity resulting from exposure to Gram-positive (*S. aureus*) and Gram-negative (*E. coli*) bacterial strains is characterized by the absence of their development on the exposed areas, also showing an inhibition zone. Following the qualitative evaluation of the powders, it was observed that all the samples determined an antibacterial effect for both bacterial strains used.

Table 5. Inhibition zone values of tested ZnO and Ag-doped ZnO powder samples (average of three values, also including sample diameter)

Sample coding	**Diameter of inhibition zone (cm)**	
	S. aureus	***E. coli***
ZnO	4.17 ± 0.12	2.30 ± 0.08
0.3% wt. Ag-doped ZnO	2.90 ± 0.08	1.77 ± 0.05
0.5% wt. Ag-doped ZnO	3.97 ± 0.11	3.03 ± 0.12
0.7% wt. Ag-doped ZnO	2.60 ± 0.08	1.47 ± 0.05

The behaviour of the samples with the used bacterial strains was different, but all the samples showed a higher antibacterial efficiency against the *S. aureus* strain, and among them, the sample of undoped ZnO has the highest efficiency, presenting the highest value of the diameter inhibition zone (4.17 ± 0.12 cm). Regarding the antibacterial efficiency against the *E. coli* strain, the best was that of the ZnO sample doped with 0.5%wt Ag, which showed the largest diameter of the inhibition zone (3.03 ± 0.12 cm).

3.5. Antifungal characterization

Antifungal activity assessed by exposure to a spore mix is characterized by the appearance of a zone of inhibition. The degree of coverage of the samples highlights the resistance of the tested samples to the action of the fungal strains.

Table 6 shows the results of the experiments regarding the antifungal efficiency of the sample powders of ZnO undoped and doped with Ag on the tested strains of fungi.

Table 6. The antifungal effect of the sample powders of undoped and Ag-doped ZnO on the tested strains of fungi (color online)

Sample coding	7 days	28 days
ZnO		
0.3% wt. Ag-doped ZnO		
0.5% wt. Ag-doped ZnO		
0.7% wt. Ag-doped ZnO		

Regarding the resistance of the analysed samples to the action of fungi, Table 7 shows the grades awarded (according to ASTM 21-09) depending on the incubation time and the degree of coverage.

Table 7. Degree of coverage of the sample powders of undoped and Ag-doped ZnO on the tested strains of fungi

Sample coding	Coverage grade			
	7 days	14 days	21 days	28 days
ZnO	0	0	2	3
0.3% wt. Ag-doped ZnO	0*	0*	0*	0*
0.5% wt. Ag-doped ZnO	0*	0*	0*	0*
0.7% wt. Ag-doped ZnO	1	1	2	3

*the presence of an inhibition zone

The samples exhibited different behaviours in response to the action of the used fungal strains. Thus, the ZnO sample showed a high resistance to the action of fungi for up to 21 days, then the resistance to the action of fungi decreased, the surface of the sample being covered up to 30-60%. Sample 0.7% Ag-doped ZnO was covered in a proportion of 10% in the first 14 days, so that at the end of the experiment, after 28 days, it reached a degree of coverage of 30-60%. After a 7-day exposure, samples 0.3% Ag-doped ZnO and 0.5% Ag-doped ZnO showed increased resistance to the action of fungi, showing an inhibition zone of approximately 1.5 cm for sample 0.3% Ag-doped ZnO and 2 cm for sample 0.5% Ag-doped ZnO (the inhibition zone also includes the sample diameter). Samples 0.3% Ag-doped ZnO and 0.5% Ag-doped ZnO kept their effectiveness and the inhibition zones from day 7, when they were first evaluated, until the end of the experimental period (28 days).

4. Conclusions

ZnO and Ag-doped ZnO nanoparticles were successfully synthesized using the sol-gel method, assisted by a surfactant (DOSS) and a gelling agent (Xylitol). All samples showed good crystallinity with a hexagonal wurtzite structure. The crystallite size increases from 34 nm (in the case of undoped ZnO) to 50.4 nm (in the case of the sample doped with 0.3% wt. Ag) but decreases with

the increase in the percentage of Ag dopant (down to 37.9 nm in the case of the sample doped with 0.7% wt. Ag). The morphology of the thus synthesized samples shown by the SEM images was similar to rods. FTIR and EDX analysis highlighted the presence of surfactant on the surface of the prepared nanoparticles. All samples showed antibacterial properties, highlighted by the inhibition zone after exposure to Gram-positive (*S. aureus*) and Gram-negative (*E. coli*) bacterial strains. The samples behaved differently, such that all the samples exposed to *S. aureus* had inhibition zones, and among them, the undoped ZnO sample had the largest diameter of the inhibition zone. Among the doped samples, the one doped with 0.5% wt. Ag showed the highest antibacterial efficiency for both bacterial strains. Also, the samples doped with 0.3 and 0.5% wt. Ag showed antifungal properties after exposure to a mixture of fungal strains; they kept their inhibition zone and the surface remained uncovered even after the final exposure period (28 days). The antibacterial and antifungal properties presented by these particles synthesized by this simple, reproducible, and efficient chemical synthesis method recommend their use as antibacterial and antifungal agents in construction materials such as cement mortars.

Acknowledgements

This work was supported by a grant of the Ministry of Research, Innovation and Digitization, CCCDI - UEFISCDI, project number PN-III-P2-2.1-PED-2021-0334, within PNCDI III.

References

[1] M. A. Maurer-Jones, I. L. Gunsolus, C. J. Murphy, C. L. Haynes, Anal. Chem. **85**(6), 3036 (2013).
[2] N. M. Shamhari, B. S. Wee, S. F. Chin, K. Y. Kok, Acta. Chim. Slov. **65**, 578 (2018).
[3] T. Malaeru, M.M. Codescu, E. Chitanu, G. Georgescu, C.A. Banciu, R.C. Dascalu, D. Patroi, V. Marinescu, I. Borbath, J. Optoelectron. Adv. M. **24**(1-2), 74 (2022).
[4] R. Wang, H. Zhang, Q. Ma, H. Niu, J. Xu, J. Optoelectron. Adv. M. **22**, 29 (2020).
[5] A. Kolodziejczak-Radzimska, T. Jesionowski, Materials **7**(4), 2833 (2014).
[6] R. Rajendran, C. Balakumar, A. Hasabo, M. Ahammed, S. Jayakumar, K. Vaideki, E. Rajesh, Int. J. Eng. Sci. Technol. **2**, 202 (2010).
[7] S. Kohzadi, A. Maleki, M. Bundschuh, Z. Vahabzadeh, S. A. Johari, R. Rezaee, B. Shahmoradi, N. Marzban, N. Amini, J. Mol. Liq. **385**, 122412 (2023).
[8] P. Dash, A. Mann, N.C. Mishra, S. Varna, Phys. E: Low-Dimens. Syst. Nanostructures **107**, 38 (2019).
[9] O. Oprea, E. Andronescu, D. Ficai, A. Ficai, F. N. Oktar, M. Yetmez, Curr. Org. Chem. **18**(2), 192 (2014).
[10] S. Shahzad, S. Javed, M. Usman, Front. Mater. **8**, 613825 (2021).
[11] R. Tülek, M. Parlak, A. Teke, J. Optoelectron. Adv. M. **25**(9-10), 459 (2023).
[12] Y. Kang, F. Yu, L. Zhang, W. Wang, L. Chen, Y. Li, Solid State ionics **360**, 115544 (2021).
[13] I. Shaheen, K. S. Ahmad, C. Zequine, R. K. Gupta, A. G. Thomas, M.A. Malik, RSC Adv. **11**, 23374 (2021).
[14] C. T. Altaf, O. Coskum, A. Kumtepe, Sci. Rep. **12**, 11487 (2022).
[15] W. Salem, D. R. Leitner, F. G. Zingl, G. Schratter, R. Prassl, W. Goessler, J. Reidl, S. Schild, Int. J. Med. Microbiol. **305**(1), 85 (2015).
[16] L. E. Shi, Z.-H. Li, W. Zheng, Y.F. Zhao, Y. F. Jin, Z. X. Tang, Food Addit. Contam. Part A **31**(2), 173 (2014).
[17] S. Muthukumaran S., R. Gopalakrishnan, Opt. Mater. **34**, 1946 (2012).
[18] S. Jurablu, M. Farahmandjou, T. P. Firoozabadi, Journal of Sciences, Islamic Republic of Iran **26**(3), 281 (2015).
[19] J. Lee, A.J. Eastealb, U. Pal, D. Bhattacharyya, Curr. Appl. Phys. **9**, 792 (2009).
[20] J. N. Hasnidawani, H. N. Azlina, H. Norita, N. N. Bonnia, S. Ratim, E. S. Ali, Procedia Chem. **19**, 211 (2016).
[21] I. B. Amor, H. Hemmami, S. E. Laouini, M. S. Mahboub, A. Barhoum, Catalysts **12**(12), 1611 (2022).
[22] X. Li, G. He, G. Xiao, H. Liu, M. Wang, J. Colloid Interface Sci. **333**, 465 (2009).
[23] E. Chitanu, C. Banciu, G. Sbarcea, V. Marinescu, A. Bara, P. Barbu (Prioteasa), Rev. Chim. **69 (**12), 3376 (2018).
[24] N. M. Shamhari, B. S. Wee, S. F. Chin, K. Y. Kok, Acta Chim. Slov, **65**, 578 (2018).
[25] B.C. Joshi, A.K. Chudhri, ACS Omega **7**, 21877 (2022).
[26] M. F. Khan, A. H. Ansari, M. Hameedullah, E. Ahmad, F. M. Husain, Q. Zia, U. Baig, M. R. Zaheer, M. M. Alam, A. M. Khan, Z. A. AlOthman, I. Ahmad, G. M. Ashraf, G. Aliev, Sci. Rep. **6**, 27689 (2016).
[27] Y. K. Tseng, M. H. Chuang, Y. C. Chen, C. H. Wu, J. Nanotechnol., **2012**, (2012), Article ID 712850.
[28] I. Limón-Rocha, C. A. Guzmán-González, L. M. Anaya-Esparza, R. Romero-Toledo, J. L. Rico, O. A. González-Vargas, A. Pérez-Larios, Inorganics **10**(2), 16 (2022).
[29] S. M. Dizaj, F. Lotfipour, M. Barzegar-Jalali, M. H. Zarrintan, K. Adibkia, Mater. Sci. Eng.: C **44**, 278 (2014).
[30] K. Ravichandran, K. Karthika, B. Sakthivel, N. Jabena Begum, S. Snega, K. Swaminathan, V. Senthamilselvi, J. Magn. Magn. Mater. **358**, 50 (2014).
[31] N. M. Khatir, Z. Abdul-Malek, A.K. Zak, A. Akbari, F. Sabbagh, J. Sol-Gel Sci. Technol. **78**(1), 91 (2015).
[32] O. Bechambi, M. Chalbi, W. Najjar, S. Sayadi, Appl. Surf. Sci. **347**, 414 (2015).
[33] S. M. Hosseini, I. A. Sarsari, P. Kameli, H. Salamati, J. Alloys Compd. **640**, 408 (2015).

*Corresponding authors: cristian.morari@icpe-ca.ro
cristina.banciu@icpe-ca.ro